Optics & Laser Technology 134 (2021) 106621

Contents lists available at ScienceDirect

Optics and Laser Technology

journal homepage: www.elsevier.com/locate/optlastec

Full length article

Bubble dynamics of laser-induced cavitation in plasmonic gold nanorod solutions and the relative effect of surface tension and viscosity

Ariana Nushin Sabzeghabae [a], Luis Felipe Devia-Cruz [b], Enoch Gutierrez-Herrera [a,c], Santiago Camacho-Lopez [b], Guillermo Aguilar [a,*]

[a] Department of Mechanical Engineering, University of California, Riverside, 92521 Riverside, CA, USA
[b] Departamento de Óptica, Centro de Investigación Científica y de Educación Superior de Ensenada, Carretera Ensenada-Tijuana No. 3918, Zona Playitas, C.P. 22860 Ensenada, B. C., Mexico
[c] Instituto de Ciencias Aplicadas y Tecnología, Universidad Nacional Autónoma de México, Ciudad de México 04510, Mexico

ARTICLE INFO

Keywords:
Gold nanoparticles
Shockwaves
Laser-induced cavitation
Laser-induced breakdown

ABSTRACT

Laser-induced cavitation (LIC) bubbles and the shockwaves they form upon collapse are destructive to nearby solid boundaries, making them of interest for biomedical and industrial applications. Furthermore, the LIC bubbles provide spatial control that can be tuned by the bubble size, collapse time and shockwave intensity. The inclusion of plasmonic nanoparticles, such as gold nanoparticles (GNP) in the liquids where LIC bubbles are formed, can further enhance the absorption of light, allowing for bubble formation at lower laser energies. However, the effect of the physical properties of such liquids on LIC bubble dynamics remains unknown. In this study, the dynamics of LIC bubbles in water–ethanol, water-glycerol, and water-GNP solutions were investigated by simultaneous high-speed shadowgraphy and spatial transmittance modulation. The first set of experiments demonstrated that LIC bubbles induced in the GNP solutions led to more efficient cavitation formation with lower fluence compared to solutions without GNPs, thereby producing higher-intensity pressure waves. A second set of experiments was conducted to determine the surface tension of GNP solutions at room temperature and was found to be 70.62 mN/m. With this information, and the corresponding values reported in the literature for ethanol and glycerol, we aimed at discerning the role of surface tension and viscosity on the dynamics of LIC bubbles, apart from the enhanced optical absorption of the GNP solutions. We observed that the optical breakdown threshold for plasma formation was reduced by 18% in GNP solutions as compared to DI water and 10.4% compared to ethanol, and the intensity of initial shockwaves in the GNP solutions was much higher than those in DI water. This enhanced intensity of shockwaves in GNP solutions compared to DI water opens a new avenue for the enhancement of cancer cell treatment and anti-bacterial applications in the biomedical field and the enhancement of the laser ablation technique in the industrial setting.

1. Introduction

Cavitation bubbles have been the main interest of many studies due to the damage they can induce to the solid boundaries in the vicinity of their formation. These bubbles can be formed mechanically, acoustically, or optically. Sometimes, this damage is a beneficial feature, (e.g. when applied to cancerous cells), which has been the focus of many biomedical applications. The cavitation bubbles presented in this paper are formed optically by tightly focusing a high-power laser beam inside a liquid, which excites the electrons through a process known as Laser-Induced Breakdown (LIB). This process initially forms a high-temperature and high-pressure plasma [1]. Electrons do not have time for acoustic relaxation, instead, mechanical relaxation occurs via propagation of a shockwave within the liquid medium and through the creation of a cavitation bubble. As the pressure inside the growing bubble decreases, the bubble collapses and another shockwave is emitted right at the end of the collapse [2–5]. Shockwaves are one of the mechanisms in laser-induced cavitation (LIC) phenomena that drive mechanical damage to solid boundaries in the close vicinity of the bubbles. Depending on the application, other phenomena such as jetting, mechanical contact, etc., are also significant contributors. Tensile stresses were observed for bubbles formed in solutions with high viscoelasticity, which is an indication of bubble behaviour in tissue-like environment is different from bubble dynamics in water [6]. The

* Corresponding author.

https://doi.org/10.1016/j.optlastec.2020.106621
Received 19 April 2020; Received in revised form 30 July 2020; Accepted 21 September 2020

intensity of shockwaves [7] directly influences the intensity of damage in applications where pressure waves have been used as a major part of treatment. These applications include eradication of various cell types, such as cancerous and Epidermal Hela cells [8,9], antibacterial effects by shockwaves [10] and cleaning surfaces of dental root canals [11].

Although plasma formation sets the initial stage of cavitation, the physical properties of the liquid influence LIC bubble dynamics at the latter stages of this process. Surface tension forces acting on LIC bubbles directly affect the growth rate and the size of the bubble [12–14]. More specifically, LIC bubbles near boundaries grow larger in solutions with lower surface tensions [14], as these solutions exhibit less resistance to deformation. Viscosity is another physical property that impacts the bubble dynamics and laser-induced shockwaves. Several studies have shown the impact of viscosity by producing cavitation in polymer solutions [15,16,6]. Knowledge of bubble dynamics and all external factors that impact them is important to researchers since the size of the LIC bubble [17] directly influences the severity of the damage on the surrounding environment. Therefore, two separate studies in water–ethanol and water-glycerol mixtures in our paper elaborate on the impact of (1) surface tension and (2) viscosity changes on LIC bubble growth, respectively.

For optical cavitation, gold nanoparticle (GNP) solutions can be used as adjuvants to enhance the damaging effects of LIC bubbles for a given laser fluence, or even reduce the fluence for equivalent damage. In particular, gold nanorods absorb more energy in the near-infrared (NIR) spectrum, which reduces the fluence requirement for plasma formation induced by a NIR laser. The optical properties of GNP solutions affect the LIB threshold and, therefore, the bubble formation threshold. However, despite the optical advantages of GNP in many applications, the lack of knowledge about the influence of physical properties on bubble dynamics extends to LIC bubbles in GNP solutions as well. More specifically, the surface tension of colloidal gold nanorod solutions and its influence on the bubble dynamics of LIC remain unknown, and the relationship between the concentration of GNP and surface tension of the solution has not been reported either. To the best of our knowledge, the only previous studies that have aimed at understanding the surface tension of GNP have used the Kelvin Equation [18,19] to calculate surface tension between the nanoparticle and vapor based on the free energy of a free nanoparticle. This concept, however, is different from the macroscopic surface tension of GNP solutions, which are the subject of our study herein. Therefore, this paper aims to address the effects of optical and physical properties of GNP solutions on the dynamics of micro- and millimetric LIC bubbles. We expect these results to allow researchers to use GNP solutions to optimize optical cavitation, particularly for biomedical applications.

2. Study design and methods

2.1. Physical and optical properties of GNP solution, water, and ethanol

The gold nanorods used in this study (C12-10-1064, Nanopartz) have a diameter and length of 10 × 66 nm and are dispersed in DI water. The GNP solution has a concentration of 4.2×10^{11} np/ml, 0.0042 wt%. The nanorods have cetyltrimethylammonium bromide (CTAB) capping agent. This coating is a cationic surfactant, which behaves as a particle stabilizer during synthesis. In all the experiments the nanoparticle solutions were sonicated for 960 s to form a homogenous mixture. The surface tension of the GNP solutions was measured using a tensiometer (SITA Dyno Tester) at room temperature. In this method, an air bubble is formed in the liquid and surface tension is measured from the forces acting on the bubble. As shown in Fig. 6c, the surface tension values of water and ethanol mixtures were obtained by values reported by Khattab et al. [20].

In order to examine the optical properties of the GNP solution, and compare the absorbance with water and ethanol, the transmission properties of the solutions in this study were obtained by an NIR spectrometer (NIRQuest, Ocean Optics). A spectroscopic cuvette (CVH100, Thorlabs) was illuminated with a white light source (HL2000 FHSA, Ocean Optics) through a fiber. Then, the transmitted light was collected through another fiber connected to the spectrometer. An average of 10 spectra and an integration time of 100 ms were chosen in these measurements.

Transmittance,$T(\lambda)$, was obtained using the following equation,

$$T(\lambda) = \frac{I(\lambda) - I_D(\lambda)}{I_0(\lambda) - I_D(\lambda)} \quad (1)$$

where I(λ) is the measured spectral intensity, $I_0(\lambda)$is the spectral intensity of light through the empty cuvette, and $I_D(\lambda)$ indicates the reference in the dark environment (Dark Spectrum).

The absorbance,$A(\lambda)$, was obtained from the calculated and normalized transmittance values by the following equation,

$$A(\lambda) = -log(T(\lambda)) \quad (2)$$

2.2. The threshold laser fluence required for bubble formation

The fluence required to form LIC bubbles is referred to as the LIB threshold. When the solution demonstrates a 50% probability of bubble formation at a certain fluence, this fluence is defined as the threshold fluence for bubble formation [21]. The plasma formation can be observed by eye since the luminescence appears as white bright light [21]. To study this phenomenon, the probability of bubble formation was obtained by sending 10 pulses at each fluence and counting the number of times the plasma was observed, then this procedure was repeated four times. The probability was reported as the average probability of four measurements for each fluence. Similarly, the error was calculated by finding the standard error between the four probabilities at each fluence.

2.3. Setup for bubble formation and analysis

The optical setup for bubble formation is shown in Fig. 1a. A Pulsed Nd:YAG laser (Surelite, Amplitude) with a pulse duration of 6 ns and wavelength of 1064 nm was used to create the bubble. A Glan-Laser polarizer and a half-wave plate were used to adjust the delivered energy. The diameter of the beam was expanded using a telescope configuration (lenses L_1 and L_2). An aspheric lens L_3 focuses the beam inside the cuvette with a focal beam waist of 14.5 μm, inducing a cavitation bubble with every pulse. A knife-edge method was used to measure the pump beam diameter at the focal point of lens L_3. A 632 nm HeNe laser continuous beam that was aimed perpendicular to the pump beam was collimated and expanded using L_4, L_5, and L_6 lenses to illuminate the bubble. The bubble appears as a dark silhouette in the high-speed camera due to the deflection of the light as shown in Fig. 1b. The evolution of bubble diameter was captured using a Phantom high-speed camera (Miro, Phantom) with a speed of 10^5 fps.

The bubbles' diameters were compared for different solutions. Bubbles were formed in the middle of the cuvette to circumvent any effect of the boundaries on the bubble dynamics. The bubble diameters were obtained by averaging the diameter four times. The Spatial Transmittance Modulation method (STM) was used simultaneously with shadowgraphy to measure the collapse time of the LIC bubbles [2]. In this method, the portions of the continuous beam that passed through the bubble are deflected, thereby, lowering the intensity of the beam that reaches the photodiode. Thus, the intensity of the light captured by the photodiode (DET 10 A, Thorlabs) in our optical setup depends on the size of the bubble, which changes with time. The intensity goes back to its initial value once the bubble collapses completely and the laser light passes undeflected. The collapse time was obtained from the photodiode data as shown in Fig. 1c. The average diameter and collapse time of five bubbles were measured for each fluence.

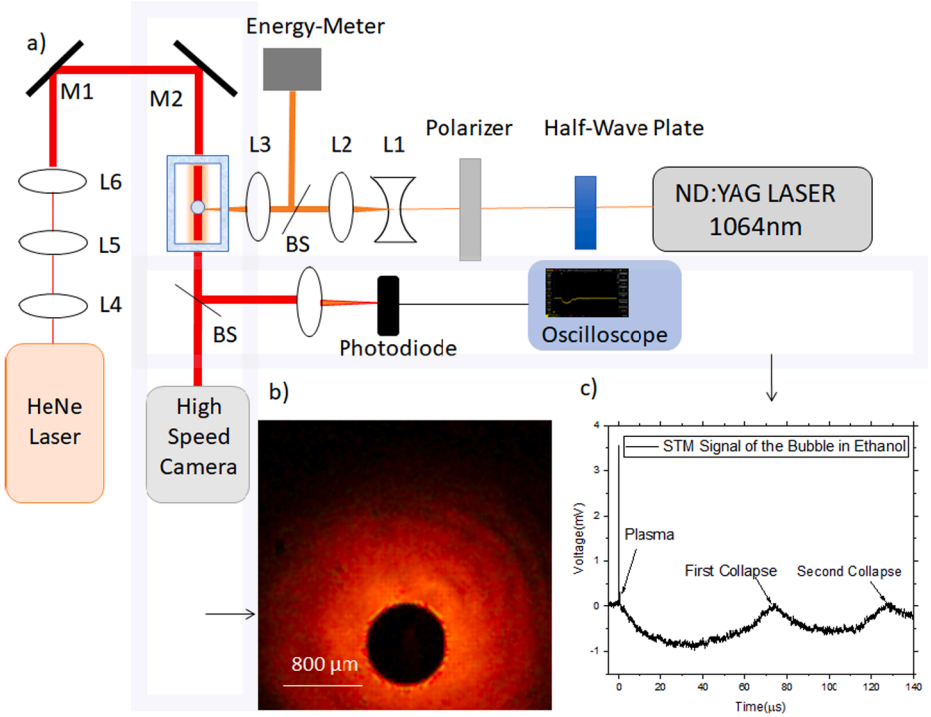

Fig. 1. (a) Optical setup for bubble formation. (b) Typical bubble image obtained by Shadowgraphy, and (c) Spatial transmittance modulation method (STM) signal is shown for a 280 J/cm^2 laser pulse.

2.4. Shockwave study

In some biomedical applications, shockwaves are the prominent damaging mechanism, which is beneficial in applications such as cancer-cell lysis, lithotripsy, dentistry and bacteria control [8–11]. In order to compare the mechanical stress induced by cavitation bubble in the medium, the comparative shockwave study between DI water, GNP solution, ethanol, and 60 wt% Glycerol-water was performed by using a Type I hydrophone with 150 ns rise time (RP Acoustics, Leutenbach Germany), which was placed initially 4 mm above the center of the bubble. The hydrophone was placed in a bag of water to avoid damage to the coating of the device. The addition of the bag around the hydrophone resulted in a 0.3 µs delay in the signal detection process. The distance between the bubble and hydrophone was modified for increments of 1.27 mm. The average of three shockwaves measurements were reported at each distance. The hydrophone was connected to a 100 MHz, 1.25 GS/s oscilloscope (TDS 3014B, Tektronix) and triggered with the pulsed laser. The amplitude of the first shockwave (the one triggered by the LIB) was compared for bubbles in all four liquids. Additionally, the Mach number for the shockwaves were obtained by moving the hydrophone away from the LIC and detecting the time that it takes for the shockwaves to reach the hydrophone at each position. Three measurements were used to obtain the average time the shockwave takes to reach the detector. By calculation the slope of position versus time plot, the Mach number was obtained.

2.5. Dynamic surface tension influence on bubble dynamics

The weight concentration of ethanol–water mixtures was modified to obtain various surface tensions from 22 mN/m to 72 mN/m using the protocols in Khattab *et al.* [20] (Fig. 6c). The surface tensions were measured by the drop number method. The experiments performed in water–ethanol solutions allowed modifying surface tension while keeping the viscosity changes minor. Additionally, water–ethanol solutions are Newtonian [22] and the viscosity remains constant at various deformation rates. For the experiments of bubble dynamics at various surface tensions, two extreme fluences were chosen and five bubbles were generated and analyzed for each concentration. The maximum bubble diameter and collapse time for each solution was correlated to the surface tension of the solutions. The errors reported in this paper were calculated by finding standard error of the five measurements.

2.6. Viscosity influence on bubble dynamics

Experiments in Newtonian [22] glycerol-water mixtures were conducted to investigate the role of viscosity on bubble dynamics. As shown in Fig. 7c, the values reported by Segar et al. [23] were used to obtain solutions with varying viscosity. It was observed that in solutions with glycerol concentrations higher than 60 wt%, there were multiple microbubbles in the solution, which affected the propagation of the laser beam due to strong light scattering and the growth of the main bubble. Therefore, concentrations below 60 wt% glycerol were selected. These experiments allowed modifying the viscosity by a factor of ten while keeping the surface tension variation minor and reducing the impact of microbubbles on the main LIC bubble [23]. The experiments in glycerol-water solutions were performed by using three different fluences. By using the optical setup shown in Fig. 1, the bubble diameter and collapse time were measured five times for each solution at every fluence. The error bars were calculated by finding the standard error of the five measurements. The optical properties of glycerol-water solutions were obtained by using water as a reference in double beam scanning UV/Vis/NIR spectrophotometer (Cary 500, Varian), which uses a high-power xenon arc lamp with wide bandwidth.

3. Results and discussion

3.1. Physical and optical properties of GNP solution, water, and ethanol

Although the surface tension of this specific type of GNP solutions has not been reported before, studies on surface tension of other nanoparticle solutions indicate that surface tension of nanoparticles solutions depends highly on the concentration, size and the material of the

nanoparticle [24–26]. Interestingly, there exists a discrepancy according to the literature in the correlation between nanoparticle concentration and the surface tension of the solutions. For example, the surface tension of nanofluids in Tanvir et al. [24] study remained unchanged at a concentration below 4 wt%. This was correlated to the low Van Der Waals forces between particles at low concentrations. A positive linear correlation between concentration and surface tension is shown for concentrations above 4 wt% [24]. In another study [25], in the case of TiO_2 nanoparticles, the surface tension decreases with increasing concentration. However, the reverse trend has been observed for FeC nanoparticle solutions [26]. For our studies, we measured the dynamic surface tension of our GNP solution (gold nanorods) with a concentration of 4.2×10^{11} np/ml, measured by tensiometer and obtained a value of 70.62 mN/m at 23.1 °C. Note that the surface tension of the solvent, DI water, is 72.2 mN/m at 23.1 °C, therefore, the presence of gold nanorods reduced surface tension of the liquid (by 2%).

NIR Spectroscopy allows a better understanding of solution absorbance at 1064 nm, which is the wavelength of the pump beam inducing the LIC bubbles. In the process of LIB, the cascade ionization is the prominent process for plasma formation. When a medium is irradiated with nanosecond pulsed laser, due to conservation of momentum, absorption of photons leads to creation and collision of free electron, which results into plasma formation once the electron density surpasses 10^{21} cm^{-3} [27]. A medium with higher optical absorbance at the pump laser wavelength can obtain the required electron density at lower energies per pulse as compared to a medium that has a lower absorbance. Therefore, the optical properties of these solutions were further investigated with the goal of better understanding the plasmonic properties of the GNP. The results indicate that water and ethanol have similar absorbance at 1064 nm (vertical line shown in Fig. 2). The absorbance of GNP solution is the highest at 1175 nm wavelength. However, the absorbance of GNP solutions at 1064 nm wavelength (the pump beam) is at least 10 times higher than the absorbance of water and ethanol. Similarly, it was previously reported that the length-to-width ratio of gold nanorods can be modified to shift the absorbance peak to the NIR desired wavelength [28]. This is a promising insight for biomedical applications, since tissue cells absorb and scatter less at NIR wavelengths [29], allowing most of the energy to get absorbed by the particles without damaging the surrounding tissue cells.

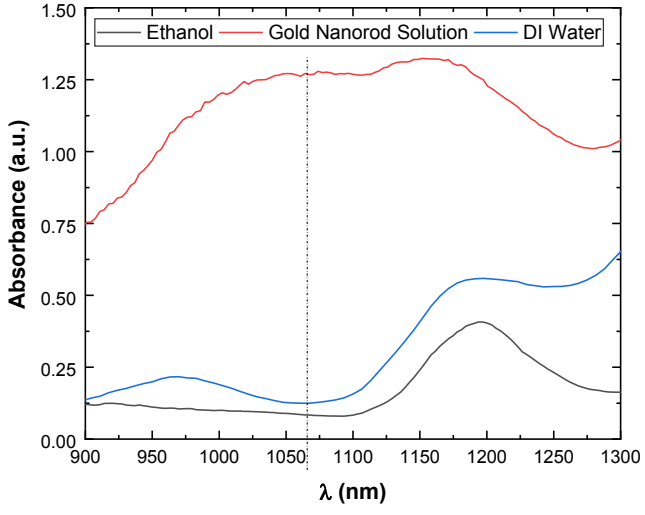

Fig. 2. NIR Spectra of the solutions at the pump beam wavelength (1064 nm), the absorbance of GNP solutions is at least 10 times higher than the absorbance of water and ethanol.

3.2. The threshold laser fluence required for bubble formation

The higher absorbance of gold nanorods solutions at 1064 nm influences the LIB threshold. To study LIB threshold, the probability of bubble formation at different fluences was measured and it is shown in Fig. 3. This probability plot describes the threshold fluence for plasma formation which then triggers bubble growth. The LIB threshold corresponds to a 50% probability of bubble formation. LIB threshold GNP strongly depends on the efficiency in optical alignment, the laser wavelength [29], the pulse duration [27]; due to these experimental differences, there exists a wide range of reported values for LIB threshold in GNP solutions.

In our study, the LIB irradiance threshold in the GNP solution was 2.75×10^{10} W/cm^2, which is comparable to the reported value of 7.8×10^{10} W/cm^2 for the LIB threshold under 6 ns pulse duration, 532 nm wavelength laser in a GNP solution [30]. According to Rau et al. [30], the breakdown threshold fluence in water is similar to the fluence required for inducing cell lysis. In our study, the LIB threshold in GNP solutions is 15% lower than the breakdown threshold in water. This indicates that using GNP reduces the fluence required to induce cell lysis. Note in Fig. 3 that, at 173 J/cm^2, no bubble is formed in water. However, GNP solution demonstrates 95% probability of bubble formation at that same fluence. The presence of GNP enhances the capacity of the medium for bubble formation even at lower fluences. The bubble-formation probability plot for GNP solutions is shifted to a lower LIB threshold (left) as compared to water and ethanol which agrees with NIR spectroscopy information (see Figs. 2 and 3). The localized heating results are caused by the plasmonic absorption features of gold nanoparticles at the resonant frequency. The free electrons in the gold nanoparticles collectively oscillate under the light illumination; this forms what is known as a localized surface plasmon and it is driven by a characteristic resonant frequency, which corresponds to an enhanced absorption at that specific wavelength. The threshold fluence for bubble formation in ethanol is lower than in water, despite ethanol having the lowest absorbance. A similar outcome was observed previously when ethanol was added to a tissue phantom. It was reported that addition of ethanol reduces the power threshold required to induce cavitation by acoustic waves. Ethanol is a volatile substance that has higher vapor pressure as compared to water, which reduced the threshold for bubble formation [31]. This effect may also be present in LIC bubbles in ethanol. GNP solutions reach from 0 the 100% probability of bubble formation within the smallest range of fluence.

Several studies have used the plasmonic properties of gold nanoparticles to enhance laser-induced nano and micro LIC bubbles and

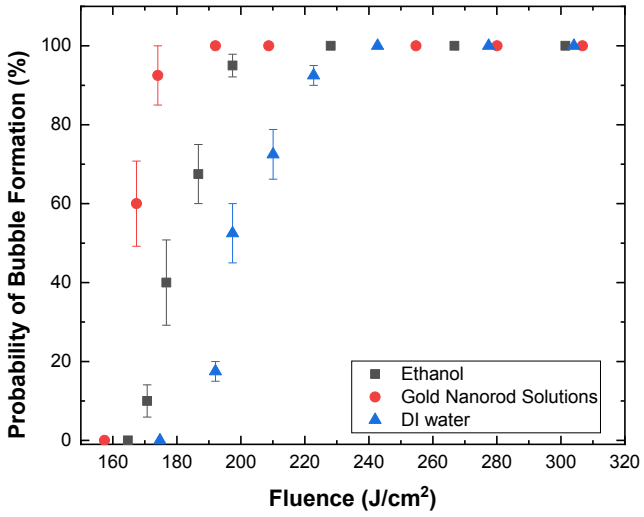

Fig. 3. Probability of bubble formation as a function of per pulse laser fluence.

rupture cell membrane, and it is known that the presence of GNP lowers the threshold energy required to damage cells [29,30,32–34] by lowering the LIB threshold, and as a consequence lowering the onset for generating LIC bubbles. The nanoparticles reduce bulk heat transfer, leading to localized heating and creation of nucleation sites. When compared to other shapes of gold nanoparticles, the accumulation of gold nanorods has shown to produce the most significant enhancement of the intensity of electromagnetic field under laser illumination [35–37].

3.3. Analysis of bubble dynamics in GNP solutions

Although the presence of GNP in solutions lowered the cavitation threshold, the bubble dynamics in GNP solutions will be further explained in this section. The bubble dynamics presented in Fig. 4a and b compare the maximum bubble diameter and collapse time in DI water, GNP solution, and pure ethanol. The bubbles in ethanol grow largest in comparison to DI water and GNP solutions because of having the lowest surface tension (Fig. 6c). The maximum bubble diameter increases as the laser fluence increases for all three solutions because at higher laser fluences, more energy is transferred to the plasma at the initial stage of bubble formation [38]. Although the absorbance of GNP solution was much higher than water and ethanol, the maximum bubble diameters in GNP solution are lower than the maximum bubble diameters in ethanol, and only slightly higher than those in DI water. This could be attributed to the energy loss due to absorption and scattering by the plasma in GNP solutions. In the GNP solution, the plasma is formed at lower frequency because GNPs provide seed electrons to start the plasma formation. The plasma forms within the leading edge of the pulse. The GNPs not only absorb but also scatter the energy in the pulse. Therefore, there is a lower effective energy spent in the bubble formation in GNP solution as compared to water and ethanol. In addition, in the GNP solution, part of the energy of the travelling pulse is absorbed by the GNPs along the optical beam path before the focal spot. These two factors can explain the lower effective energy transformation to create a bubble in the GNP solution.

The collapse time of the bubbles is another factor that characterizes the bubble dynamics. The STM technique allows a more accurate measurement of collapse time than the use of high-speed photography. Using STM traces we studied the growth and collapse of the bubbles. The bubbles in water have the highest surface tension, so they exhibit the shortest lifetime. In contrast, the bubbles in the solutions with the lowest surface tension (i.e. ethanol) have the longest lifetimes. The lifetime of bubbles in GNP solutions were slightly longer than those in water.

3.4. Shockwave study

Despite the higher absorbance of the GNP solution compared to DI water (Fig. 2), the maximum bubble diameter and collapse time of bubbles in GNP solutions are not significantly higher than bubbles formed in water (Fig. 4a and b). This could be due to higher scattering rates in GNP solutions and the transfer of the energy to production of the initial shockwave, since the initial shockwave forms prior to the bubble [5]. The intensity of shockwave in GNP solutions was compared to the intensity of the shockwave in DI water, ethanol, and 60 wt% Glycerol-water solutions in Fig. 5a and b. The amplitudes of shockwaves in GNP solutions were higher than in water. This result indicates that GNP in solution allow lowering the fluence requirements to induce similar damage to the surrounding environment compared to cells without nanoparticles. Similarly, our results confirm that higher intensity of damage can be obtained when GNP are used. Surprisingly, the shockwaves in glycerol-water solutions have the highest shockwave intensity compared to the rest of the solutions. We attribute this to the damping effects in highly viscous solutions, in which the shockwaves carry out its energy over a longer distance, Fig. 5b. According to Vogel et al, [39] the shockwave energy loss is the highest close to the plasma, with 85–90% energy loss within the 200–300 μm from the focal point. Therefore, in our far-field shockwave measurements, the energy dissipation over distance impacts the shockwave measurements as well.

Another study [40] in various glycerol-water solutions indicated that the intensity of shockwaves is the lowest for solutions with the highest glycerol concentration. However, their results also indicated that shockwaves Mach number decays at a lower rate over distance for solutions with higher glycerol concentration. Therefore, at a distance of 300 μm away from the LIC, the solution with 100% wt. glycerol concentration has the highest Mach number despite having the lowest initial shockwave pressure. Therefore, in our far-field measurements, the higher intensity of shockwaves in glycerol-water solution, Fig. 5b, is due to lower dissipation rate in solutions with higher viscosity. In order to confirm this result, we also investigated Mach number as a function of glycerol concentration as shown in Fig. 5c. As the glycerol concentration (viscosity) increases, the average speed of the shockwave increases. Liquids with lower viscosity such as water have higher dissipation rate, therefore by the time the shockwave reaches the hydrophone, the shockwave has lost the majority of its energy resulting in smaller Mach numbers. Gold nanoparticles solution and ethanol had Mach numbers equal to 4.31 and 3.37, respectively.

Our results also indicate that shockwaves in ethanol have the lowest intensity at far distance from the source d > 4 mm, Fig. 5a and b. This

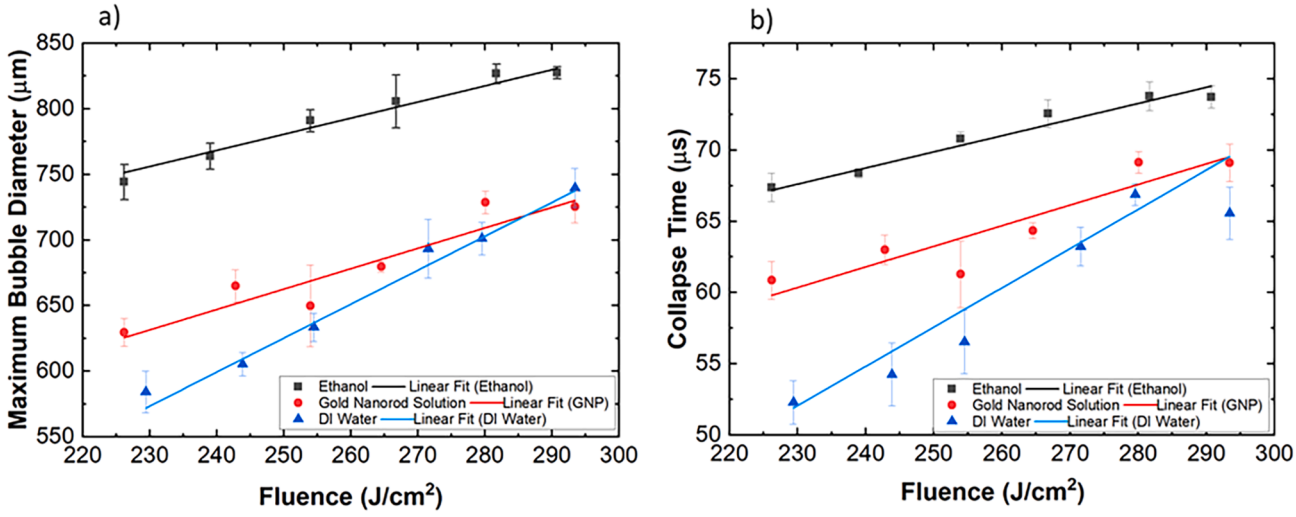

Fig. 4. (a) Maximum bubble diameter vs. fluence for the three solutions is shown. (b) Collapse time vs. fluence for the three solutions.

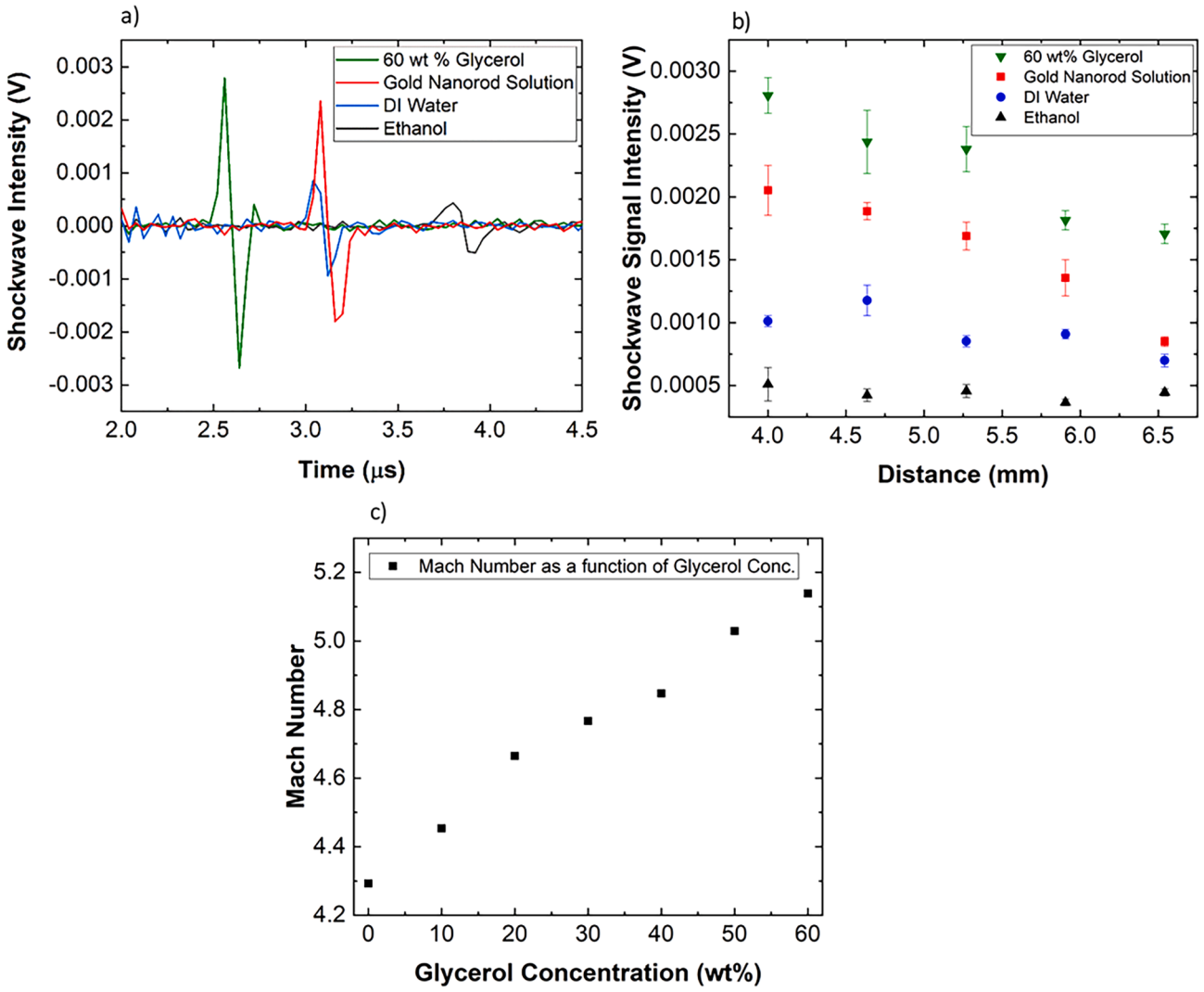

Fig. 5. (a) Typical shockwave signal distribution over time at a distance 5.3 mm away from the bubble. This data was smoothed by Origin. (b) Shockwave intensity at various distances from the LIC in water, GNP solutions, 60 wt% glycerol, and ethanol. (c) The shockwave Mach number as a function of concentration for pressure waves formed in various glycerol solutions.

can be an indication of higher dissipation rate or lower shockwave pressures at the initial stages. Additionally, the bubbles were bigger in ethanol compared to bubbles in water and GNP solutions. Further confirming that more laser energy is transferred to bubble formation and thus less energy is transferred to acoustic energy resulting in lower intensity shockwaves in ethanol.

3.5. *Surface tension influence on bubble dynamics*

A set of experiments in ethanol–water solution with various ethanol concentration was conducted to investigate the impact of surface tension on bubble dynamics. As shown in Fig. 6c, the relative concentration in ethanol–water solutions is directly correlated to the surface tension of these solutions. However, the viscosity also changes as ethanol concentration varies and the secondary impact of viscosity changes is also explained in more in details in this section. The surface tension of water is high due to the hydrogen bonds. Therefore, as the concentration of water in water–ethanol solutions decreases, the surface tension also decreases. As the surface tension decreases, the maximum bubble diameter becomes larger, Fig. 6a. A polynomial trend with a negative leading coefficient was used to extrapolate results between data points. The inertial force on the bubble must overcome the surface tension while the bubble is growing in the medium.

In Fig. 6a and b the bubble diameter and collapse time vs. surface tension are plotted, respectively. In both graphs, as the surface tension increases, weight concentration of ethanol decrease (refer to Fig. 6c). As the surface tension forces acting on the bubble increases in the solutions with lower ethanol content, the bubble diameter decreases. However, the collapse time does not follow the same trend as seen in Fig. 6b. The explanation for this phenomenon is rooted in viscosity variations shown in Fig. 6c. For solutions with surface tension between 30.11 and 72 mN/m (ethanol concentration 44.13 to 0 wt%), viscosity decrease with increase in surface tension. Yet, for solutions with surface tensions below 30.11 mN/m, viscosity increase as surface tension increases.

For solutions with surface tension between 30.11 and 72 mN/m, as viscosity decreases and surface tension increases, and the maximum bubble diameter decreases as well, Fig. 6a. This means that the reduction in viscosity has relatively lower impact on bubble diameter than surface tension since the opposite trend would have been expected due to viscosity changes. Therefore, the increase in surface tension has a bigger role on bubble diameter and bubbles grow smaller. Both decrease in viscosity and increase in surface tension in this region contribute to decrease in the collapse time, Fig. 6b in this region.

For solutions with surface tension between 22 and 30.11 mN/m (100 to 44.13 wt% ethanol concentration), the viscosity is increasing as surface tension increases. If surface tension is increasing, collapse time

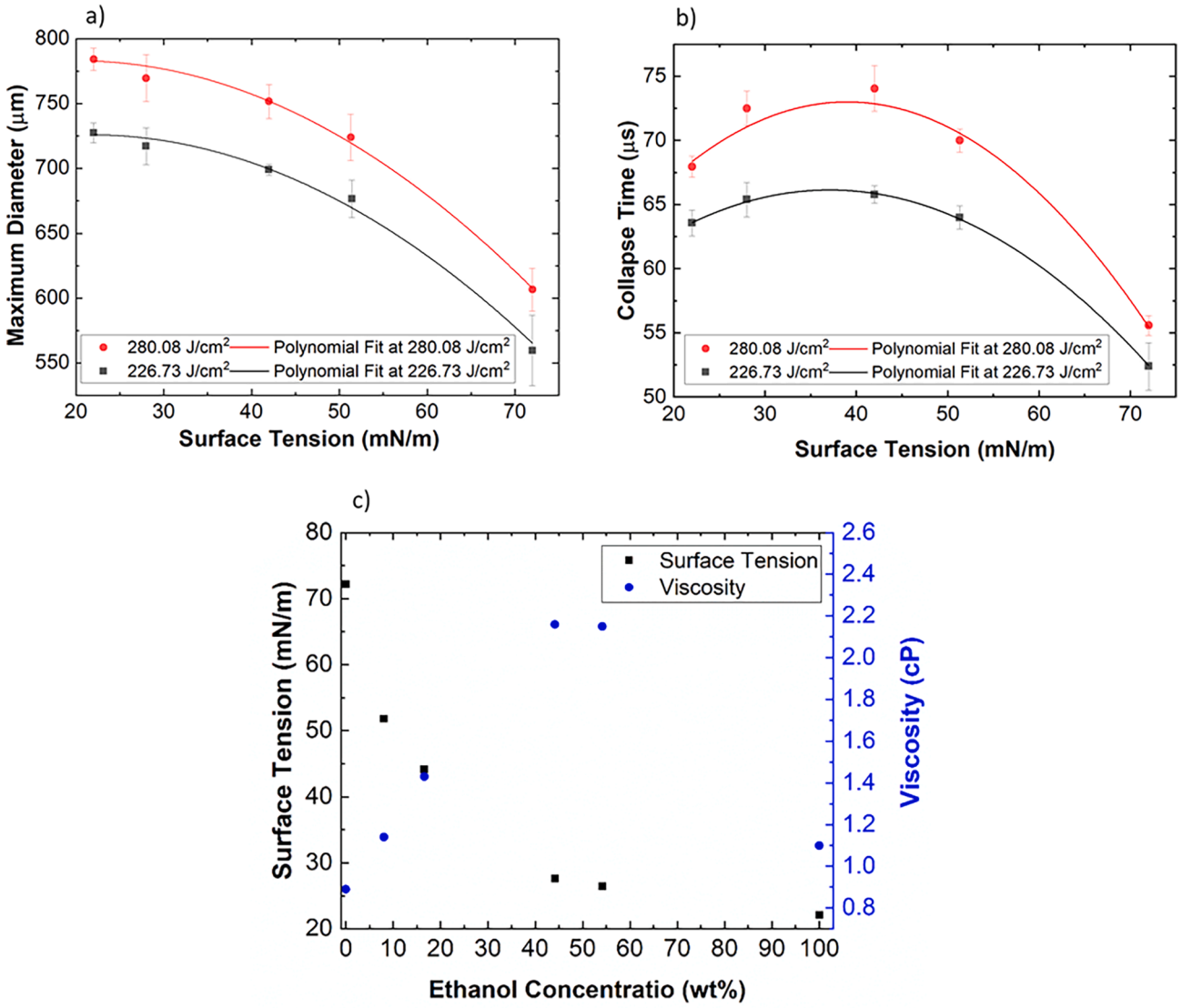

Fig 6. (a) Maximum diameter of the bubbles in ethanol–water solutions with various surface tension (i.e. ethanol concentrations). (b) Collapse time of the bubbles in ethanol–water solutions with various surface tension (i.e. ethanol concentrations). (c) Correlation between surface tension and viscosity variation with ethanol concentration is reported based on results in Khattab et al. [20].

should decrease because the bubbles grow smaller and the bubble takes less time to collapse. However, in this region, the opposite occurred. The collapse time is increasing despite the bubbles growing smaller. This result is because of the increase in viscosity in this region. This indicates that the drastic increase in viscous forces in solutions with surface tension from 22 to 30.11 mN/m, has a bigger impact on collapse time than changes in surface tension.

There are several studies on the relationship between surface tension and bubble dynamics. Liu et al. [14] calculated LIC bubble dynamics near boundaries from the collapse times measured using the optical beam deflection method. However, the authors only focus on examining ethanol, pure water and solutions with similar surface tensions, and did not study the solutions with surface tensions between the two extremes. In another study, the correlation between surface tension and cavitation behaviour was explained theoretically [13]. In that study, acoustic cavitation with 1 m/s growth rate was considered. The cavitation behaviour was unaffected by change in surface tension of the liquid for large bubbles. However, it was reported that for smaller bubbles, the surface tension effect on bubble diameter increases. The LIC bubbles formed in our study have around 20 times faster growth rate than acoustic bubbles in the paper mentioned above. Due to rapid plasma formation in our study, it is expected that the inertial forces are higher in LIC bubbles as compared to bubbles formed acoustically. Therefore, the interaction between the inertial force and the surface tension force has a bigger impact on the dynamics of the bubbles than the ones observed for acoustic cavitation.

3.6. *Viscosity influence on bubble dynamics*

To investigate the role of viscosity on bubble dynamics even further, bubbles in glycerol-water solutions were compared to bubbles in DI water. By increasing the glycerol concentration from 0 to 60 wt%, the viscosity changes exponentially from 1.005 cp to 10.8cp [23], while the surface tension varies only slightly from 72 mN/m to 68 mN/m [41]. Therefore, the experiments in glycerol-water solutions allow keeping surface tension changes minor, in contrast to the water–ethanol mixture. The maximum bubble diameter increases rapidly when viscosity increases from 1.15 to 3 mPa·s. At viscosities higher than 3 mPa·s the rate of change of maximum bubble diameters in solutions decrease for all laser fluences, see Fig. 7a. By increasing the concentration of glycerol, not only viscosity increases exponentially, the absorbance of glycerol-water solutions at 1064 nm increases as well, refer to Fig. 7c. In

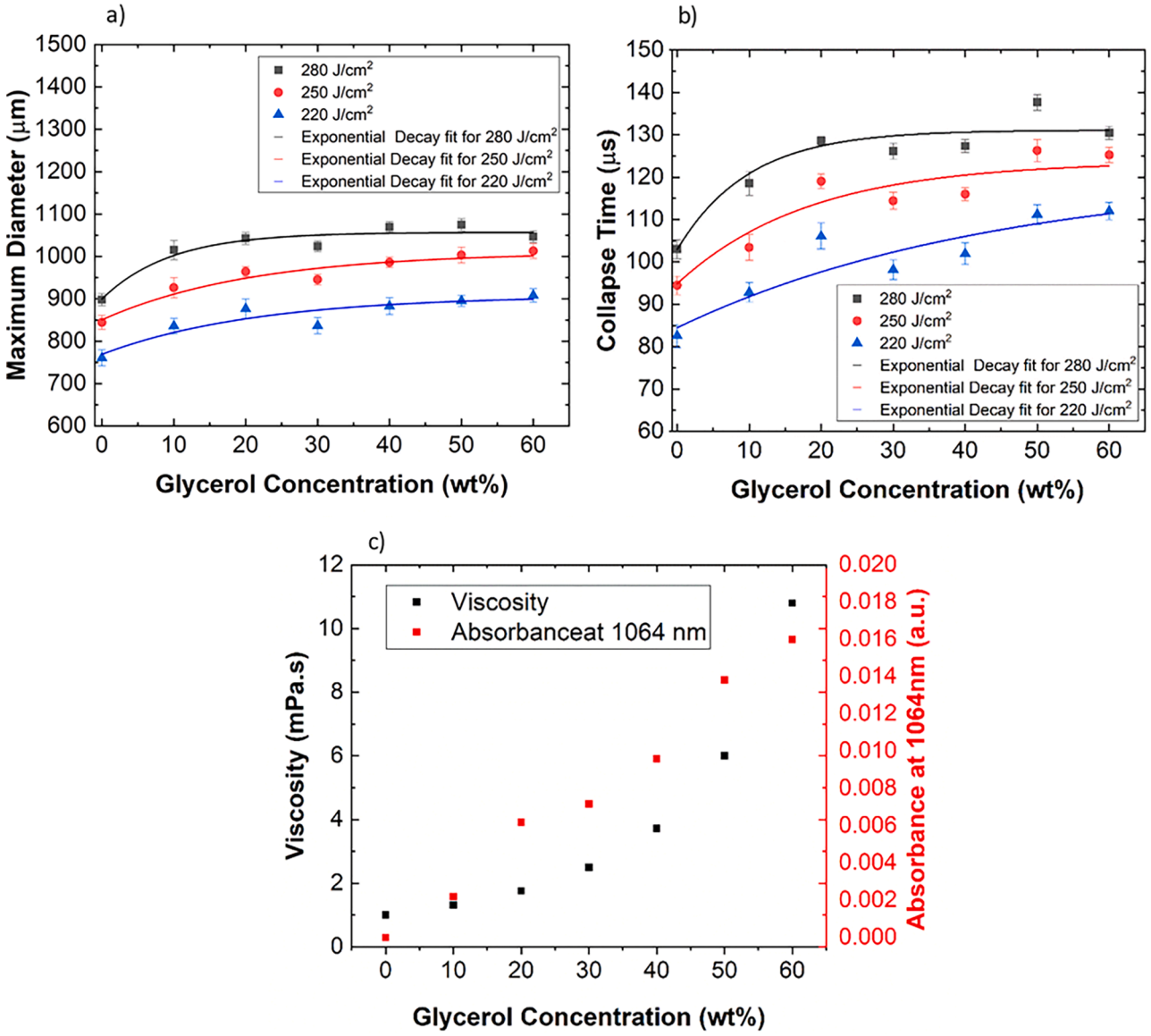

Fig. 7. (a) Maximum diameter of the bubbles in glycerol-water solutions with various concentrations. (b) Collapse time of the bubbles in glycerol-water solutions with various concentrations. (c) NIR absorbance of glycerol-water solutions with reference to DI water and viscosity values reported by Segar et al. [23] as a function of glycerol concentration.

highly viscous solutions, viscous forces acting on the bubble will resist the bubble growth in the medium, therefore the bubble should not grow as big. Concurrently, in our glycerol experiments, such solutions have higher absorbance at the wavelength used to create the plasma (1064 nm). Solutions with high absorbance at 1064 nm, should produce bigger bubbles due to the higher strength of the plasma and high electron density at the cavitation site. These two phenomena are occurring simultaneously in Fig. 7a and b. Viscosity changes at a slower rate for lower concentrations due to exponential relationship between viscosity and glycerol concentration. Therefore, at lower concentrations, the impact of absorbance seems to surpass the impact of viscosity. Once the concentration is above 30 wt%, viscosity and absorbance effects on maximum bubble diameter seem to neutralize each other and no significant changes in bubble diameter is observed.

Similarly, the collapse time increases drastically when increasing the concentration of glycerol from 0 to 20 wt%. However, for concentrations above 30 wt%, the rate of change in collapse time versus glycerol concentration depends on the energy used to induce the bubble, as Fig. 7b shown. For bubbles formed by the highest energy of 280 J/cm^2 in Fig. 7a and b, the changes in collapse time are within the measurement uncertainty.

However, the collapse time of bubbles formed with lower fluences continues to increase by increasing the glycerol concentration. The bubble dynamics do not change once the absorbed fluence surpasses a certain threshold (refer to discussion of Fig. 4a and b). This phenomenon explains the plateau in the curve for bubbles formed by 280 J/cm^2 laser pulse. For lower fluence, the increase in absorbance alongside increase in viscosity for higher glycerol concentrations lead to higher collapse times.

The average speed of the bubble–liquid interface can also be analyzed from Fig. 7a and b by dividing the average maximum bubble diameter by the average time it takes the bubble to reach its maximum size. The time it takes for the bubble to reach the maximum bubble diameter is half of the collapse time based on the symmetric nature of the STM signal (Fig. 1c). When viscosity changes from 1.005 mPa·s (DI water) to 10.8 mPa·s (60 wt% glycerol), the speed of the bubble–liquid interface reduces from 18.43 m/s to 16.22 m/s for bubbles formed by 280 J/cm^2 laser pulse. The ten times increase in viscosity increases the

resistance of the fluid to deformation under tensile stress, therefore the bubble growth rate slows down.

There exists a discrepancy between reports that studied LIC bubbles in glycerol solutions by using a 1064 nm pulsed laser. Liu et al [42] described the decline of the bubble size to be only 25 μm after changing viscosity from 0 to 50 cP, and the increase of bubble lifetime was only 5 μs. Another study indicated that an increase in concentration of glycerol from 0 to 100% does not change the main bubble dynamics significantly; however, the plasma luminescence intensity highly depends upon the concentration of glycerol [43]. It remained unknown why by changing the viscosity, the bubble diameters remained unchanged or decreased only slightly. Brujan et al [15] also investigated the effect of viscoelasticity on bubble dynamics by comparing water to solutions with polymer additives. The polymer additives increased the viscosity and elasticity of the solutions. They reported that as the laser energy increases the impact of rheology on the bubble oscillation time diminishes. However, for laser energies below the threshold energy, the bubble radius is smaller in polymer solutions compared to water. Similarly, in our experiments with higher laser energies, the curves in Fig. 7a and b reach the plateau at lower concentrations, indicating the reduction of viscosity effects on bubble dynamics. Although from 0 to 30 wt% glycerol, our result shows an increase in bubble diameter and collapse time, we attribute the discrepancy between our study and Brujan et al [15] due to use of glycerol instead of polymers to change the viscosity of the solutions and different bubble sizes. In a separate study performed by Brujan et al [16], the effect of viscosity on bubble diameter for bubbles above 0.5 mm was not as prominent as compared to smaller bubbles in their other study [15]. Contrastingly, Li et al [42] also investigated the bubble dynamics in glycerol-water solutions in order to examine the impact of viscosity and showed bubble diameters and collapse time change due to the addition of glycerol, even for larger bubbles with diameters above 0.8 mm. In our study, we measured the bubble diameter by using a high-speed camera, instead of computing the bubble diameter from the collapse time or simulation like in some of the other works. In the reports mentioned above, the higher optical absorption of glycerol when compared to water at 1064 nm wavelength was overlooked. In our study, the bubbles grow slightly larger in solutions with higher glycerol content. This effect occurs despite the increase in viscous forces acting on the bubble in solutions with higher glycerol content. Higher viscosity should reduce the maximum bubble diameter, however as the concentration of glycerol increases, the absorbance and viscosity increase simultaneously. More energy is transferred to the bubbles in solutions with higher absorbance, therefore the bubbles will increase in size due to this effect. At the same times, the solutions with higher glycerol concentrations also have higher viscosity which resist the bubble growth and increase the damping and collapse time of the bubble. These two effects happen simultaneously and as a result the changes in bubble diameter are not significant. Our study also indicates that by changing the glycerol concentration from 0 to 60 wt%, the collapse time increases by 30% while the bubble diameter only increases by 10%. This result demonstrates that glycerol concentration highly influences the collapse time more than it does to the maximum bubble diameter. Higher absorbance and viscosity of solutions with high glycerol content both lead to bubbles with longer collapse times.

In summary, researchers can use the results reported in this paper to tailor the properties of GNP solutions and obtain the desired outcome in biomedical and industrial applications. According to the literature, bubble size [17] and shockwave intensity [7] impact the severity of damage induced to the surrounding by the LIC. For instance, to obtain a larger damage area, higher intensity of shockwave and bubble diameter should be used, which can be obtained by the addition of GNP and reduction of the surface tension of the solvents, respectively. Additionally, the use of GNP allows a more precise damage mechanism since lower laser fluence is required. Lastly, the speed of LIC process can be tuned by changing the viscosity of the solvents. Bubbles with slower speed and growth rate will form in highly viscous solutions.

4. Conclusions

The presence of GNP increased the shockwave intensity as compared to water, however the diameter and collapse time of bubbles in GNP solutions only altered slightly compared to the bubbles formed in water. GNP provide seed electrons and enhance the transformation of the energy for creation of the plasma. On the other hand, due to scattering of GNP, there is less energy efficiency in bubble formation process, therefore the bubble diameters do not change significantly. The surface tension of GNP- DI water solutions was measured, and we observed addition of gold nanoparticles to DI water reduces the surface tension slightly. Although water–ethanol solutions were initially used to study the surface tension of the liquids, we must note that there also exists some variation in viscosity in these solutions, impacting the maximum radius and collapse time during the cavitation process. Another study in glycerol-water solutions was conducted and showed that the increase in viscosity was correlated to longer collapse times of bubbles. The overall findings of this study indicate that physical properties of solutions (surface tension and viscosity) allow researchers to control the cavitation dynamics, therefore better managing the intensity of the damage to the surrounding. Also, GNP lower the energy required to induce cavitation and shockwave production resulting more localized damage and efficient cavitation process.

CRediT authorship contribution statement

Ariana Nushin Sabzeghabae: Conceptualization, Methodology, Writing - review & editing, Writing - original draft, Visualization, Investigation. **Luis Felipe Devia-Cruz:** Conceptualization, Methodology, Investigation, Writing - review & editing. **Enoch Gutierrez-Herrera:** Conceptualization, Methodology, Writing - review & editing. **Santiago Camacho-Lopez:** Conceptualization, Methodology, Writing - review & editing, Resources. **Guillermo Aguilar:** Conceptualization, Methodology, Writing - review & editing, Supervision, Project administration, Resources.

Declaration of Competing Interest

The authors declare that they have no known competing financial interests or personal relationships that could have appeared to influence the work reported in this paper.

Acknowledgments

The authors of this paper would like to thank Dr. Robert Zenit and Bernardí Palacios for their assistance with surface tension measurements and most specially, Mr. David Halaney, for helping with the discussion and editing of the paper. ANS and GA acknowledge the support of the National Science Foundation (NSF:PIRE 1545852) and Department of Education (GAANN P200A180037).

References

[1] A. Vogel, J. Noack, G. Huttman, G. Paltauf, Mechanism of femtosecond laser nanosurgery of cells and tissues, Appl. Phys. B 81 (2005) 1015–1047.
[2] L. Devia-Cruz, S. Camacho-Lopez, R. Evans, D. Garcia-Casillas, D. Stepanov, Laser-induced cavitation phenomenon studied using three different optically-based approaches - An initial overview of results, Photon Lasers Med. 1 (3) (2012) 195–205.
[3] W. Lauterborn, A. Vogel, Shock Wave Emission by Laser Generated Bubbles, Bubble Dyn. Shockw. 8 (2012) 67–103.
[4] M.K. Bhuyan, A. Soleilhac, M. Somayaji, T.E. Itina, R. Antoine, R. Stoian, High fidelity visualization of multiscale dynamics of laser-induced bubbles in liquids containing gold nanoparticles, Sci. Rep. 8 (2018) 1–12.
[5] R. Evans, S. Camacho-Lopez, F.G. Perez-Gutierrez, G. Aguilar, Pump-probe imaging of nanosecond laser-induced bubbles in agar gel, Opt. Express 10 (2008) 7481–7492.
[6] E.A. Brujan, A. Vogel, Stress wave emission and cavitation bubble dynamics by nanosecond optical breakdown, J. Fluid Mech. 558 (2006) 281–308.

[7] E.A. Brujan, Shock wave emission from laser-induced cavitation bubbles in polymer solutions, Ultrasonics 48 (2008) 423–426.
[8] R. Dijkink, S. Le Gac, E. Nijhuis, A. Berg, I. Vermes, A. Poot, C. Ohl, Controlled cavitation–cell interaction: trans- membrane transport and viability studies, Phys. Med. Biol. 53 (2008) 375–390.
[9] L.B. Jr Feril, T. Kondo, Z. Cui, Y. Tabuchi, Q. Zhao, H. Ando, T. Misaki, H. Yoshikawa, Umemura, Apoptosis induced by the sonomechanical effects of low intensity pulsed ultrasound in a human leukaemia cell line, Cancer Lett. 221 (2) (2005) 145–152.
[10] G. Divya Prakash, R.V. Anish, G. Jagadeesh, D. Chakravortty, Bacterial transformation using micro-shockwaves, Anal. Biochem. 419 (2011) 292–301.
[11] N. Lukac, M. Jezersek, Amplification of pressure wave in laser-assisted endodontics with synchronized delivery of Er:YAG laser pulses, Lasers Med. Sci. 33 (2018) 823–833.
[12] Y. Iwai, S. Li, Cavitation erosion in waters having different surface tensions, Wear 254 (2003) 1–9.
[13] E. Samiei, M. Shams, R. Ebrahimi, A novel numerical scheme for the investigation of surface tension effects on growth and collapse stages of cavitation bubbles, Eur. J. Mech. B/Fluids 30 (2011) 41–50.
[14] X.M. Liu, J. He, J. Lu, X.W. Ni, Effect of surface tension on a liquid-jet produced by the collapse of a laser-induced bubble against a rigid boundary, Opt. Laser Technol. 1 (2011) 21–24.
[15] E.A. Brujan, Shock wave emission and cavitation bubble dynamics by femtosecond optical breakdown in polymer solutions, Ultrason.-Sonochem. 58 (2019) 1–8.
[16] E.A. Brujan, P.R. Williams, Cavitation Phenomena in Non-Newtonian Liquids, Chem. Eng. Res. Des. 84 (2006) 293–299.
[17] M.S. Huston, X. Ma, Plasma and Cavitation Dynamics during Pulsed Laser Microsurgery in vivo, Phys. Rev. Lett. 99 (2007), 158104-1–158104-4.
[18] K.K. Nanda, A. Maisels, E. Kruis, Surface Tension and Sintering of Free Gold Nanoparticles, Phys Chem 112 (2008) 13488–13491.
[19] S.C. Vanithakumari, K.K. Nanda, Phenomenological Predictions of Cohesive Energy and Structural Transition of Nanoparticles, J. Phys. Chem. B 110 (2006) 1033–1037.
[20] I.S. Khattab, F. Bandarkar, M.A. Abolghasemi Fakhree, A. Jouyban, Density, viscosity, and surface tension of water+ethanol mixtures from 293 to 323K, Korean J. Chem. Eng. 6 (2012) 812–817.
[21] B. Varghese, V. Bonito, M. Jurna, J. Palero, M.H.R. Verhagen, Influence of absorption induced thermal initiation pathway on irradiance threshold for laser induced breakdown, Biomed. Opt. Express 6 (4) (2015) 1234–1240.
[22] C. Ayela, L. Nicu, Micromachined piezoelectric membranes with high nominal quality factors in Newtonian liquid media: A Lamb's model validation at the microscale, Sens. Actuators, B 123 (2007) 860–868.
[23] J.B. Segur, H.E. Oberstar, Viscosity of glycerol and its aqueous solutions, Ind. Eng. Chem. 9 (1957) 2117–2120.
[24] S. Tanvir, L. Qiao, Surface tension of Nanofluid-type fuels containing suspended nanomaterials, Nanoscale Res. Lett. 7 (2012) 1–10.
[25] S.M. Sohel Murshed, S. Tan, N. Nguyen, Temperature dependence of interfacial properties and viscosity of nanofluids for droplet-based microfluidics, J. Phys. D Appl. Phys. 41 (2008) 1–5.
[26] A. Huminic, G. Huminic, C. Fleaca, F. Dumitrache, I. Morjan, Thermal conductivity, viscosity and surface tension of nanofluids based on FeC nanoparticles, Powder Technol. 284 (2015) 78–84.
[27] J. Noack, A. Vogel, Laser-Induced Plasma Formation in Water at Nanosecond to Femtosecond Time Scales: Calculation of Thresholds, Absorption Coefficients, and Energy Density, IEEE J. Quantum Electron. 35 (8) (1999) 1156–1167.
[28] X. Huang, M.A. El-Sayed, Gold nanoparticles: Optical properties and implementations in cancer diagnosis and photothermal therapy, J. Adv. Res. 1 (2010) 13–28.
[29] M. Kitz, S. Preisser, A. Wetterwald, M. Jaeger, G.N. Thalmann, M. Frenz, Vapor bubble generation around gold nanoparticles and its application to damaging of cells, Biomed. Opt. Express 2 (2) (2011) 291–304.
[30] K.R. Rau, P.A. Quinto-Su, A.N. Hellman, V. Venugopalan, Pulsed Laser Microbeam-Induced Cell Lysis: Time-Resolved Imaging and Analysis of Hydrodynamic Effects, Biophys. J. 1 (2006) 317–329.
[31] C. Chen, Y. Liu, S. Maruvada, M. Myers, D. Khismatullin, Effect of ethanol injection on cavitation and heating of tissues exposed to high-intensity focused ultrasound, Phys. Med. Biol. 57 (2012) 937–961.
[32] Y. Arita, M. Ploschner, M. Antkowiak, F. Gunn-Moore, K. Dholakia, Laser-induced breakdown of an optically trapped gold nanoparticle for single cell transfection, Optical Society of America 38 (17) (2013) 3402–3405.
[33] C.M. Pitsillides, E. Joe, X. Wei, R.R. Anderson, C.P. Lin, Selective Cell Targeting with Light-Absorbing Microparticles and Nanoparticles, Biophys. J . 6 (2003) 4023–4032.
[34] V.P. Zharov, R.R. Letfullin, E.N. Galitovskaya, Microbubbles-overlapping mode for laser killing of cancer cells with absorbing nanoparticle clusters, J. Phys. DAppl. Phys. 38 (2005) 2571–2581.
[35] L. Tong, Y. Zhao, T. Huff, M. Hansen, A. Wei, J. Cheng, Gold Nanorods Mediate Tumour Cell Death by Compromising Membrane Integrity, Adv. Matter. 19 (2007) 3136–3141.
[36] H. Xiaohua, I.H. El-Sayed, W. Qian, M.A. El-Sayed, Cancer Cell Imaging and Photothermal Therapy in the Near-Infrared Region by Using Gold Nanorods, J. Am. Chem. Soc. 128 (2006) 2115–2120.
[37] O. Ekici, R.K. Harrison, N.J. Durr, D.S. Eversole, M. Lee, A. Ben-Yakar, Thermal Analysis of Gold Nanorods Heated with Femtosecond Laser Pulses, J. Phys. D Appl. Phys. 41 (2008), 185501-1–185501-11.
[38] M. Mohammadzadeh, S.E. Gonzalez-Avila, K. Liu, Q.J. Wang, C.-D. Ohl, Synthetic jet generation by high frequency cavitation, J. Fluid Mech. Rapids 823 (2017). R3-1–R3-12.
[39] A. Vogel, J. Noack, K. Nahen, D. Theisen, S. Busch, U. Parlitz, D.X. Hammer, G. D. Noojin, B.A. Rockwell, R. Birngruber, Energy balance of optical breakdown in water at nanosecond to femtosecond times scales, Appl. Phys. B 68 (1999) 271–280.
[40] H. Kurahara, K. Ando, Effects of Liquid Viscosity in Laser-induced Shockwave Dynamics, ASME Proceeding 5 (2019).
[41] F. Behroozi, J. Smith, W. Even, Effect of viscosity on dispersion of capillary-gravity waves, Wave Motion 48 (2011) 176–183.
[42] X.M. Liu, J. He, J. Lu, X. Ni, Effect of Liquid Viscosity on a Liquid Jet Produced by the collapse of a Laser-Induced Bubble near a Rigid Boundary, Jpn. J. Appl. Phys. 48 (2009), 016504-1–016504-5.
[43] E.M. Englert, A. McCarn, G. Williams, Luminescence from laser-induced bubbles in water-glycerol mixtures: Effect of Viscosity, Phys. Rev. E 83 (2011), 046306-1–046306-5.